Effect of Y$_2$O$_3$ Nanoparticles on the Evolution of the Microstructure and Mechanical Properties of Severely Plastic Deformed Cu Sheets During Friction Stir Processing

Mohammad Amin Yaghoubi[1] · Nozar Anjabin[1,2] · Hyoung Seop Kim[2,3]

Abstract

Pure Cu sheets with severe plastic deformation were obtained using constrained groove pressing (CGP) and subjected to different passes of friction stir processing (FSP) with and without yttria nanoparticles. The fine grain structure of the CGP-treated samples underwent rapid grain growth during 1-pass FSP without nanoparticles. The addition of yttria particles resulted in a very fine-grained structure in the stir zone (SZ) with a high hardness value and the lowest weight loss during the wear test. Applying 3 passes of FSP resulted in homogeneous dispersion of reinforced particles in both the annealed and CGP processed samples. The SZ of the sample that was processed with CGP and 3-pass FSP in the presence of yttria had a finer grain with higher strength and wear resistance than the FSP-treated annealed samples.

1 Introduction

The application of severe plastic deformation (SPD) techniques for the development of ultrafine-grained materials has attracted much attraction during the last two decades [1]. Among various SPD techniques, constrained groove pressing (CGP) is suited for plate-shaped materials [2]. In the CGP technique, samples undergo large shear deformation by alternate pressing with a set of grooved and flat dies [3]. This technique was successfully used to process various metallic materials such as pure Cu and Al alloy sheets.

✉ Nozar Anjabin
  Anjabin@shirazu.ac.ir

✉ Hyoung Seop Kim

1 Department of Materials Science and Engineering, School of Engineering, Shiraz University, P.O. Box: 71348-51154, Shiraz, Iran

2 Graduate Institute of Ferrous and Energy Materials Technology, Pohang University of Science and Technology (POSTECH), Pohang 37673, Republic of Korea

3 Department of Materials Science and Engineering, Pohang University of Science and Technology (POSTECH), Pohang 37673, Republic of Korea

Krishnaiah et al. [4] showed that by applying 1-pass CGP, the yield strength of pure Cu was increased from 70 MPa at the annealed condition to 220 MPa. They also reported that the average hardness increased from 44 VHN at the annealed condition to about 99 VHN for the sample processed by 3-pass CGP, the grain size decreased from an initial value of 78 μm to about 41 μm, and a cell structure with the approximate size of 0.5 μm was achieved [5]. Another study reported that by imposing two passes of the CGP process on an annealed Cu sheet the hardness, yield strength, and ultimate tensile strength were increased about 70%, 225%, and 25%, respectively [6]. This microstructure refinement and enhanced mechanical properties appear to be related to the dislocation cell structure formation and transferring cell walls to high-angle grain boundaries [7].

On the other hand, some studies focused on developing surface particulate composites using friction stir processing (FSP) to overcome the problem of low hardness and wear properties of Cu components. Barmouz et al. [8, 9] employed FSP to manufacture Cu/SiC surface composites. The composite layer possessed finer grain size with enhanced hardness and wear resistance than pure Cu. They also found that the lower traverse speed resulted in a more uniform dispersion of SiC microparticles in the SZ, which

further reduced the grain size and produced a higher hardness [8]. Moreover, they reported that employing multi-pass FSP improved the distribution of particles and reduced the size of the grain and SiC particles in the SZ, which created higher microhardness and enhanced tensile properties [9]. Raju et al. [10] investigated the influence of the Al_2O_3 microparticles fraction and process parameters on the mechanical properties of copper surface composites made by FSP. The results showed that tensile properties were improved by increasing the volume percent of reinforced particles due to the dislocation movement retardation and the increase in the recrystallization temperature. Sabbaghian et al. [11] and Akramifard et al. [12] employed FSP to manufacture Cu-based surface composites reinforced with TiC and SiC particles, respectively. They found that the composite layer had higher microhardness with better wear resistance than the base metal (BM), due to the presence of particles and the grain refinement in the SZ. Moreover, they reported that no intermetallic compounds were formed during FSP. Khosravi et al. [13] used FSP to produce Cu/WC surface composites. The composite sample had higher hardness than pure copper and increased hardness by raising the rotational speed and the number of FSP passes. Ahn et al. [14] fabricated a Cu/B_4C surface composite by FSP, proving that the presence of B_4C particles during FSP causes the formation of a very fine grain structure in the SZ with improved hardness. Dinaharan et al. [15] developed a TiB_2 particle reinforced Cu-based surface composite using FSP and found that many of the TiB_2 particles were fractured during FSP and the composite samples had a very fine grain with enhanced hardness and wear resistance. Dinaharan et al. [16] also investigated the effect of reinforcing particle types including SiC, Al_2O_3, B_4C, and TiC on the microstructure, microhardness, and wear behavior of Cu composites fabricated by FSP. They observed that for all types of particles, the composite samples had a finer grain size with remarkably higher wear resistance than pure copper and that there was no interfacial reaction between the copper and the reinforcements. Avettand-Fènoël et al. [17] used FSP to incorporate yttria particles into copper to make a Cu surface composite. They showed that after multiple passes of FSP, the initially added micron-size particles were fragmented into different size classes from the micrometric to the nanometric scale, and as the number of FSP passes increased the particle dispersion became more homogeneous. The composite samples had higher strength and work hardening capacity than those in the BM.

In the above-mentioned studies, FSP was performed on conventionally grained copper, and no study was done on FSP of ultrafine-grained copper. However, there is some published research on friction stir welding (FSW) of different SPD-treated samples, such as accumulated roll boned (ARBed) Al 1100 [18], equal channel angular pressed (ECAPed) Al 1050 [19], ECAPed Al 2024 [20], ARBed low carbon steel [21], CGPed pure aluminum [22], and dissimilar joining of CGPed copper and CGPed aluminum [23]. According to these studies, FSW of SPD-treated materials may decrease mechanical properties in the SZ compared to those in the BM because of recrystallization and grain growth phenomena driven by high stored energy from the SPD process and heat generation during FSW [24].

Khorrami et al. [25–27] investigated the effect of SiC nanoparticles on the FSP of Al sheets previously subjected to severe plastic deformation by CGP. According to their results, SZ hardness decreased during FSP without nanoparticles because of the instability of the SPD structure, which undergoes large grain growth. However, the addition of SiC nanoparticles restricted grain growth by pinning the grain boundary during recrystallization, which created a finer grain size with higher hardness than the sample that was FSPed without particles [25]. They also investigated the effect of the number of passes on particle distribution and found that clusters of nanoparticles formed on the retreating side (RS) of the SZ during the first and second passes of FSP, causing a brittle fracture in tensile testing. However, a higher number of passes produced well-distributed nanoparticles, which created a finer grain structure in the SZ [26]. Moreover, they showed that performing FSP at cryogenic temperature improves mechanical properties in both SZ and HAZ of composite samples [27].

Considering the above literature survey, there are limited research works concerning the manufacturing of surface composite on SPD-treated samples, and there is no published study on FSP of copper with severely plastic deformation. Hence, the aim of our study was to investigate the influence of adding yttria nanoparticles during FSP on the properties of CGP-treated copper sheets. To do so, pure copper sheets processed by 4 passes of CGP were subjected to 1 and 3 passes of FSP with and without yttria nanoparticles. The microstructure, mechanical properties, and wear resistance behavior of samples were investigated and compared to those of the annealed samples.

2 Material and Methods

As-received commercial pure copper (C11000) sheets of 3 mm thickness were cut into square samples of 50 mm length and annealed at 650 °C for 2 h. Then, some of the specimens were subjected to SPD, employing 4 passes of CGP with a die groove angle of 45° and groove width of 3 mm. The CGP-treated and annealed samples were subjected to FSP with a shoulder with a 16 mm diameter, and a cylindrical tool pin with a 3 mm diameter and 2 mm height. The tool tilt angle was selected to be 2.5°. For the composite samples, 10 holes were drilled on the top surface of the specimens with a depth and diameter of 2 mm (Fig. 1a).

Then, the holes were filled with yttrium oxide particles with a diameter of 50–70 nm (Fig. 2). FSP was performed at a constant rotation of 1600 rpm and travel speed of 20 mm/min.

Microstructural characterization was carried out using optical microscopy (OM), and the mean grain size was determined using ImageJ. To do so, a transverse cross-section of the processed samples was prepared by mechanical grinding and polishing and then etched with 65% HNO_3. The distribution of yttria was observed using OM and scanning electron microscopy (SEM) with energy dispersive X-ray spectroscopy (EDX) analysis. The hardness of the processed region was measured using the Vickers microhardness tester with a load of 25 g and a dwell time of 15 s. A uniaxial tensile test was performed at room temperature with a constant ram velocity of 1 mm/min on a longitudinal specimen prepared according to ASTM E8 with a gauge length of 12.5 mm (Fig. 1b). The wear behavior of the samples was investigated through a pin-on-disk wear test with a load of 1 kg, sliding speed of 0.03 m/s, and sliding distance of 250 m. The worn surface was investigated using SEM.

3 Results and Discussion

3.1 Microstructure of Base Metal

Figures 3a and b show the microstructure of the BM in the annealed and CGP-treated conditions, respectively. In Fig. 3a, the annealed sample shows an equiaxed grain structure with a mean grain size of 56 μm, and some annealing twins can be observed. As shown in Fig. 3b, the SPD-treated structure contains elongated grains with a mean grain size of 7.7 μm. This grain refinement along with the high dislocation density accumulated in the samples during 4 passes of CGP with an equivalent strain of 4.46 has resulted in an increase in hardness from 66 HV for the annealed sample to 135 HV in the CGPed one.

3.2 Microstructure of 1-Pass FSPed Samples: with Y_2O_3 Particles

Figure 4a shows the OM image of the transverse cross-section of the annealed sample after 1-pass FSP. The SEM images and the results of EDX elemental mapping analysis for the A_1 through A_3 regions of Fig. 4a are presented in Figs. 4b and c, respectively. As can be seen from these figures, the distribution of yttria nanoparticles is not homogeneous and many particles are aggregated in the RS, resulting in a large agglomeration of yttrium oxide. During FSP, the plasticized material flow in a vortex motion from the advancing side (AS) to the RS [28], hence the nanoparticles are transferred from the AS to the RS, resulting in

inhomogeneous particle distribution. Despite the higher fraction of nanoparticles in the RS, the grain size of the SZ in the AS is not finer than that of AS. This reveals that due to the agglomeration of particles in the RS, the nanoparticles cannot effectively pin the grain boundary and so grain growth occurred in this region.

The OM image of the transverse cross-section of the CGP-treated sample after 1-pass FSP is presented in Fig. 5a. As this figure shows, some tunnel defects are present on the AS, which may be related to the insufficient flow of materials during FSP [29, 30]. Due to the large accumulated strain resulting from 4 passes of CGP, the material flow stress is increased. Hence, the material flow during subsequent FSP is decreased compared to the annealed sample and leads to the formation of tunnel defect. The SEM micrograph of the tunnel defects at the AS is also presented in Fig. 5a with the corresponding EDX analysis. These figures reveal many yttria nanoparticles agglomerated in tunnel defects. However, from SEM images presented in Fig. 5b, it is observed that the distribution of nanoparticles is relatively homogeneous in other regions (A_1–A_4) than the annealed sample. Comparing the EDX elemental map analysis presented in Figs. 4c, and 5c also proves that the distribution of yttria particles in the CGP-treated sample is more uniform than the annealed one. Moreover, according to Fig. 5a, the grain size in the RS of the CGP-treated sample is finer than that of the annealed sample.

3.3 Microstructure of 3-Pass FSPed Samples: with Y_2O_3 Particles

Figures 6a and b show the microstructure of the transverse cross-section of annealed and CGPed samples after 3-pass FSP. The EDX elemental maps for the region marked in Fig. 6a are depicted in Fig. 7. Also, the EDX analysis results for the same region in the 1-pass processed annealed sample are presented in this figure for comparison. As can be seen, by increasing the number of FSP passes, the large agglomerates of nanoparticles that appeared in the 1-pass FSPed sample are fragmented, and a more homogeneous distribution is achieved in the annealed sample. Comparing the results presented in Figs. 6b and 5a, it is evident that the tunnel defect formed during 1-pass FSP in the CGPed sample is completely removed after 3-pass FSP. Moreover from Figs. 6a and b, it is observed that the grain size of the SZ in the CGPed sample is finer than the annealed one because the severe strain imposed by the CGP process results in a very fine grain structure with a high fraction of grain boundaries, which can serve as a preferred site for nucleation of dynamic recrystallization [31].

Fig. 1 a Schematic of the
FSP setup used in this work **b**
Schematic showing the location
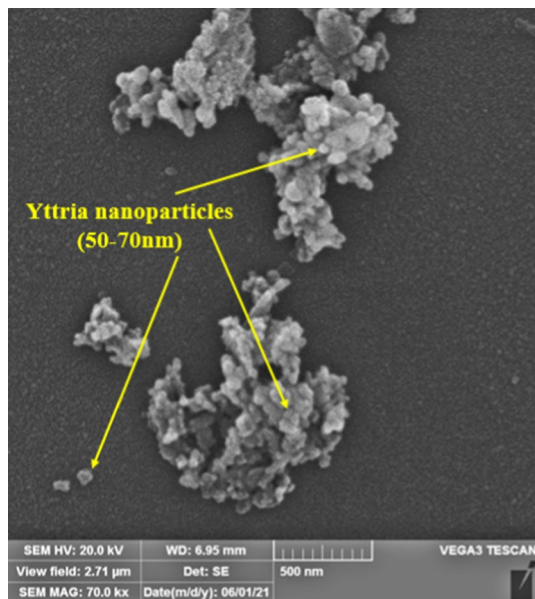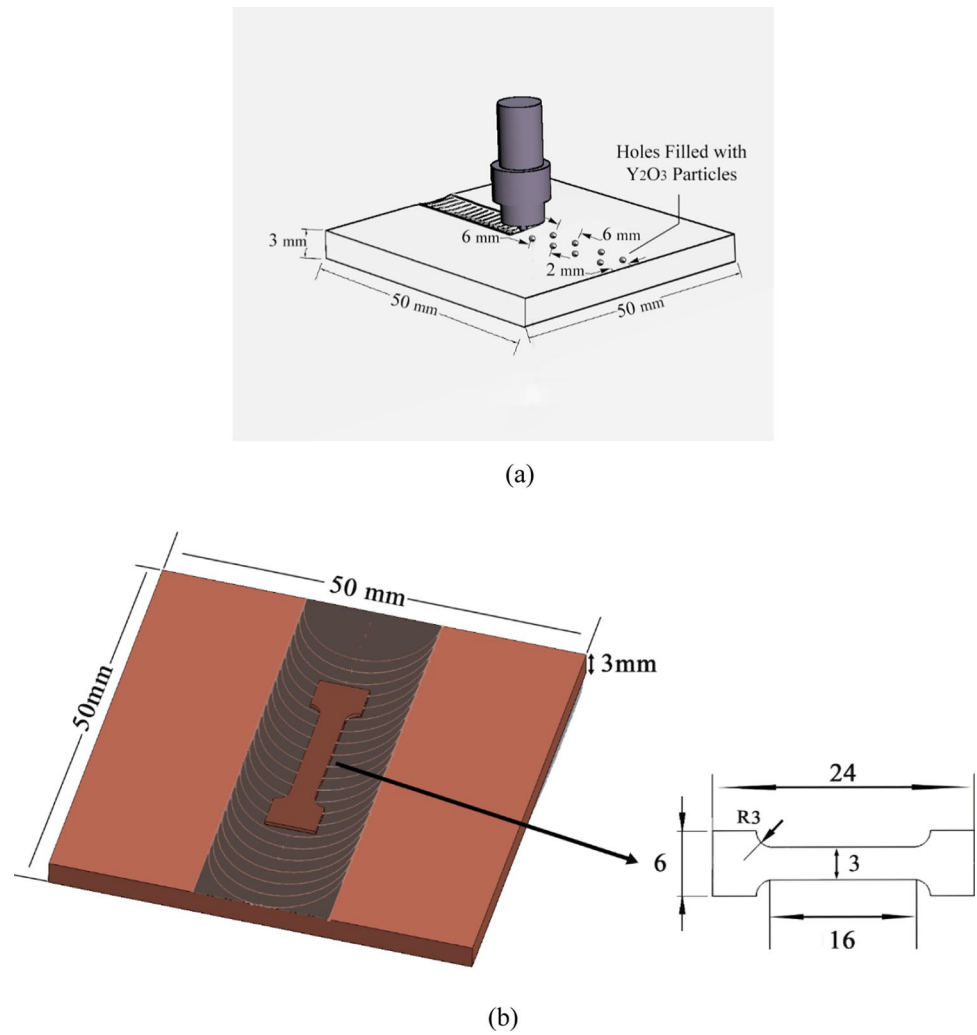and dimension of the tensile test
specimen

(a)

(b)

Fig. 2 SEM micrograph of yttrium oxide nanoparticles

3.4 Comparison of the Microstructure of FSPed Samples: with and Without Y_2O_3 Particles

Figure 8 shows the SZ microstructure of the annealed sample subjected to 1 and 3 passes of FSP with and without Y_2O_3 nanoparticles. In Fig. 8a, it can be seen that the 1-pass FSPed sample without yttria particles has a finer grain size (12 μm) than the corresponding base metal (56 μm). This is due to the dynamic recrystallization during thermomechanical treatment of FSP, resulting in a fragmentation of the initial annealed grain into finer grains [12]. Comparing Figs. 8a and b shows that by increasing the number of FSP passes, the SZ grain size decreases because of the more plastic deformation and higher heat input received during multiple passes of FSP. As can be seen in Fig. 8c, adding nanoparticles during 1-pass FSP of the annealed sample does not change the grain structure of the SZ due to the agglomeration of the nanoparticles in the RS, which cannot effectively retard the grain growth. According to Fig. 8d, the addition of nanoparticles leads to the formation of a
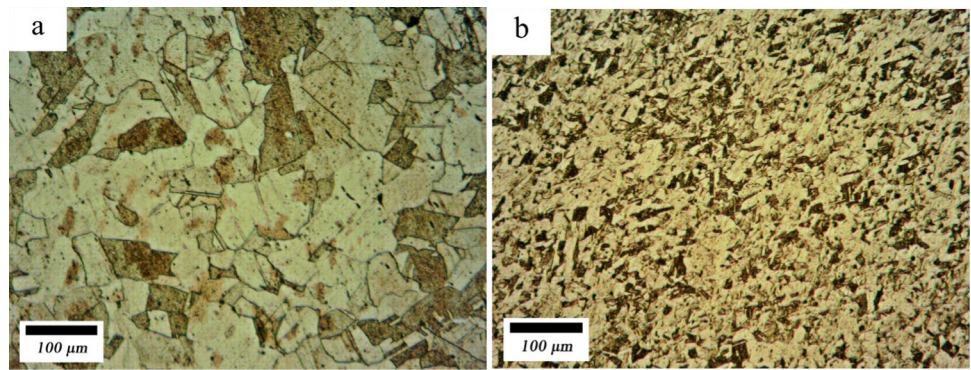
homogeneous grain structure in the 3-pass FSPed sample, which is related to the suitable distribution of nanoparticles at a higher number of FSP passes and their pinning effects on the grain boundary. However, the average grain size of the 3-pass FSPed samples with yttria is almost the same as that of the samples processed without nanoparticles.

Figure 9 shows the microstructure of the CGP-treated sample after different numbers of passes of FSP with and without yttria nanoparticles. Moreover, the mean grain size of the annealed and CGPed samples after FSP is given in Table 1. According to these results, the SZ in the CGPed sample after 1-pass FSP contains a larger grain size than the corresponding BM (Fig. 3b). The high strain energy stored in the copper during CGP results in an unstable structure that undergoes grain growth due to thermomechanical treatment applied in FSP and leads to the formation of large grains in the SZ. It can also be seen that the SZ microstructure of the 3-pass FSPed sample consisted of much finer equiaxed grains than that of the 1-pass processed sample. In fact, the stored energy resulting from the CGP process was released during the first pass of FSP, and at a higher number of passes of FSP grain refinement occurred. A similar result was also reported for the grain structure evolution in a SPD-treated Al during multiple FSP passes [26]. As is seen in Fig. 9c, adding yttria nanoparticles during 1-pass FSP results in a very fine grain structure. Although during the first pass of FSP in the CGPed sample, a large fraction of nanoparticles accumulated in tunnel defects on the AS, the remaining particles had a relatively uniform distribution in the SZ (Fig. 5b). Therefore, nanoparticles can effectively limited grain boundary movement and created a fine grain structure. Moreover, compared to the annealed sample, in the CGP-treated specimen, there are more grain boundaries that can serve as nucleation sites and lead to a finer grain structure than in the annealed sample [31]. According to Fig. 9d, the CGPed sample after 3 passes of FSP in the presence of yttria nanoparticles contains very fine grains (0.6–1 µm). This grain refinement is due to the more homogeneous dispersion of nanoparticles at a higher number of passes of FSP, resulting in an improvement of grain boundary pinning [26].

3.5 Hardness

Figure 10 presents the average hardness of the SZ for the CGP-treated and annealed samples after various passes of FSP. The SZ hardness for the annealed sample is higher than the corresponding BM. As discussed earlier, during FSP of the annealed samples, dynamic recrystallization occurs, which causes the grain size to decrease and the dislocation density to increase, leading to a higher hardness value. Adding yttria during the first FSP pass did not have much effect on the hardness of the annealed sample because many nanoparticles accumulated in the RS, resulting in an inadequate pining effect. The CGPed sample after 1-pass FSP without nanoparticle had lower hardness than the corresponding BM. As mentioned earlier, the microstructure of the CGPed sample was unstable and rapid grain growth occurred during the first pass of FSP, so a lower hardness value than in the CGPed BM was obtained. In the present study, Y_2O_3 nanoparticles were added during FSP to improve the mechanical properties of the SZ by retarding grain growth. As shown in Fig. 10, in the presence of nanoparticles, the SZ hardness of the CGPed sample even after 1-pass FSP has considerably increased compared to the sample processed without nanoparticles due to the retarding the grain growth process and creation of a homogeneous and fine grain structure. Increasing the number of FSP passes leads to a higher value of hardness in both the annealed and CGPed samples. This improvement is the result of a competition between two processes: (a) at a higher number of FSP passes, the material undergoes more plastic deformation and therefore more grain refinement occurs [26], and (b) the time the material is exposed to heating increases, which causes more grain growth after dynamic recrystallization. According to Fig. 10, by adding nanoparticles during FSP the hardness is improved for both the annealed and CGPed samples. This enhancement is due to the pinning effect of nanoparticles on grain boundary movement, which delays grain growth, and to the Orowan strengthening effects.

Fig. 4 **a** Macrograph of the transverse cross-section of the annealed sample after 1-pass FSP, and OM images at higher magnification from AS and RS, and **b**, **c** SEM images and EDX elemental map analysis of yttrium element for A_1–A_3 regions marked in Fig. 4a
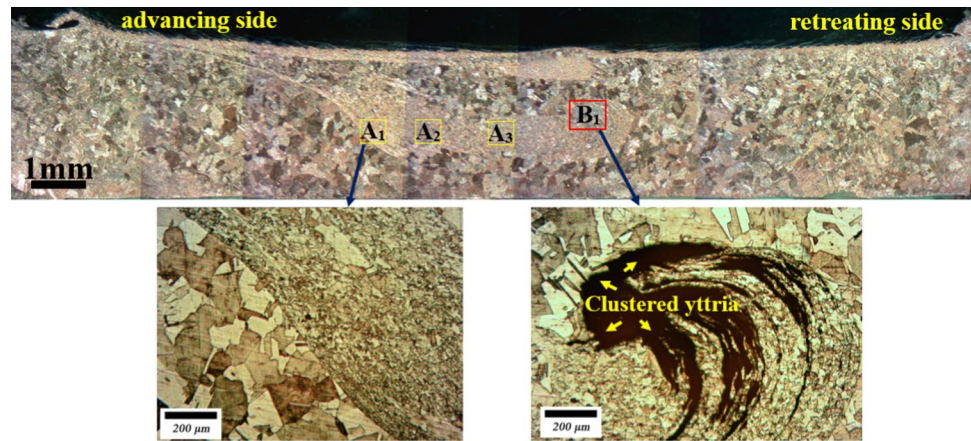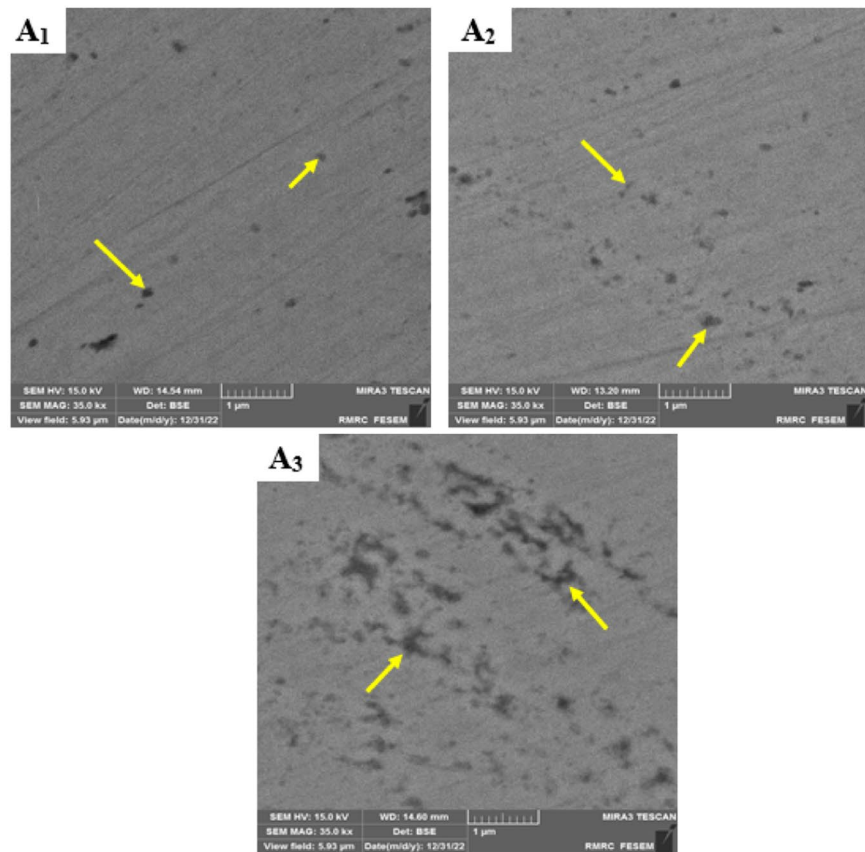

3.6 Tensile Test

Engineering stress–strain curves for the annealed and CGP-treated samples before FSP and after 3 passes of FSP are shown in Fig. 11. The mechanical properties of samples taken from Fig. 11, are summarized in Table 2. It can be seen that the unprocessed annealed sample has the highest value of elongation and the lowest yield strength (YS) and ultimate tensile strength (UTS) because, during the annealing process, an equiaxed grain structure with low internal stress is formed. Applying 3 passes of FSP on the annealed sample increases the YS and UTS, which is due to the strengthening resulting from the dislocation density increment and grain refinement. An increase in material strength during FSP was also reported in earlier studies for different materials, such as copper [32], brass [33], and aluminum [34]. The addition of nanoparticles to the annealed sample during FSP causes a small increase in the YS with a slight decrease in UTS and

Fig. 4 (continued)

(c)
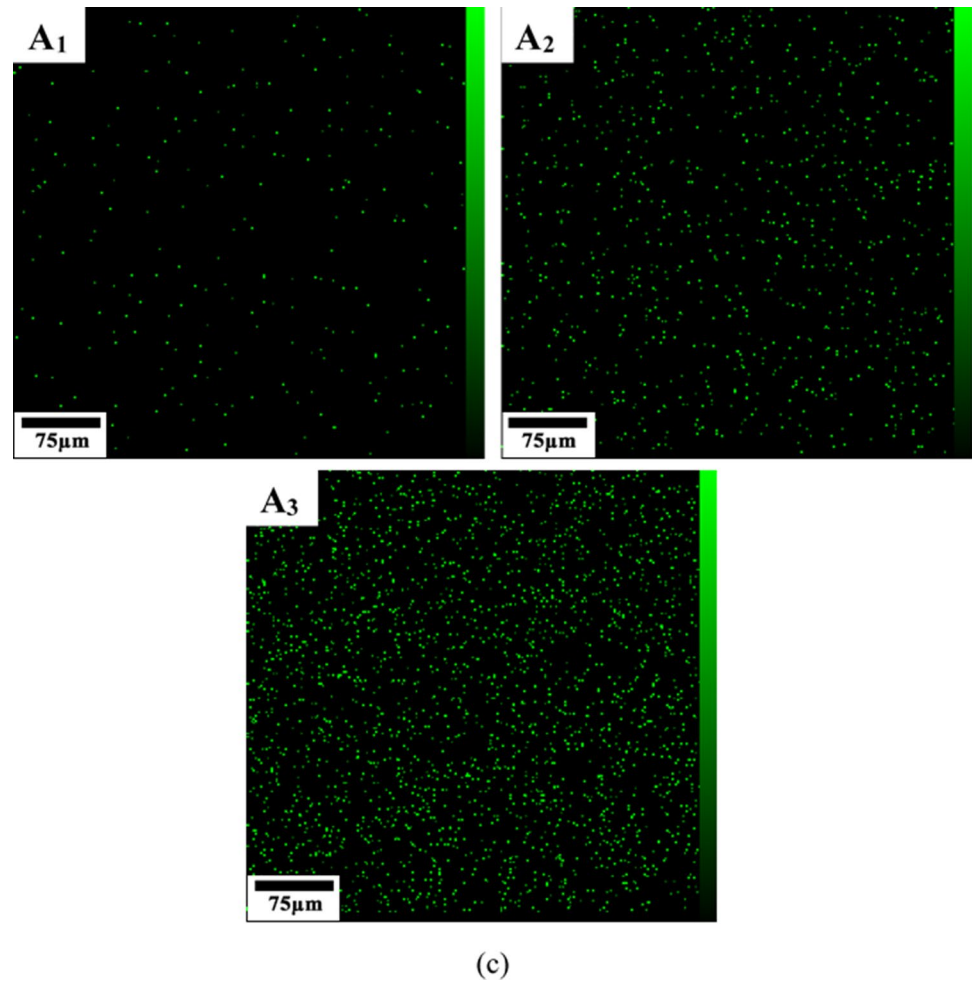
a relatively large reduction in elongation. This adverse effect of particles on the tensile properties of the surface composite may be related to the crack initiation susceptibility at the interfacial region between the particles and metal matrix, as well as the high local stress concentration caused by the presence of hard particles. In general, the strength of a composite depends on different parameters such as the bonding between particles and matrix, dislocation density, and grain size. While the pining effect of nanoparticles on the grain boundary and the Orowan strengthening mechanism which increased the dislocation storage rate during the deformation process enhances the material strength, the weak bond and the stress concentration created by the particles can reduce the tensile properties [17, 35].

The unprocessed CGPed sample had high strength with low elongation, which was due to the accumulation of high dislocation density and grain refinement during SPD [36]. By applying 3 passes of FSP, the strength of the CGP-treated sample decreased while elongation increased compared to the BM. During the first pass of FSP, the high

dislocation density and internal stress developed during CGP were annealed out, and the subsequent grain growth reduced the strength. At a higher number of FSP passes, the fragmentation of grains by dynamic recrystallization produced a very finer grain structure with a strength much higher than that of the 1-pass FSPed sample. However, the strength of the 3-pass FSP-treated sample was still lower than that of the CGPed BM. By the addition of yttria nanoparticles, the strength of the CGP-treated sample after 3-pass FSP increased compared to the CGPed BM because of an increase in the dislocation storage rate and retardation of grain boundary movement.

In Fig. 11, the elongation of the CGP-treated sample is significantly lower than the annealed one. This was related to the low strain hardening capacity of the CGPed structure, which was due to a high amount of dislocation density and the weak interaction of dislocations due to the short mean free path of dislocation movement in the CGP-treated microstructure [36]. By performing FSP, the elongation of the CGPed sample increased, while it decreased for the annealed

Fig. 5 **a** Macrograph of the transverse cross-section of the CGPed sample after 1-pass FSP, SEM image, EDX analysis, and OM image at higher magnification from RS, and **b**, **c** SEM images and EDX elemental map analysis of yttrium element for A_1–A_4 regains marked in Fig. 5a
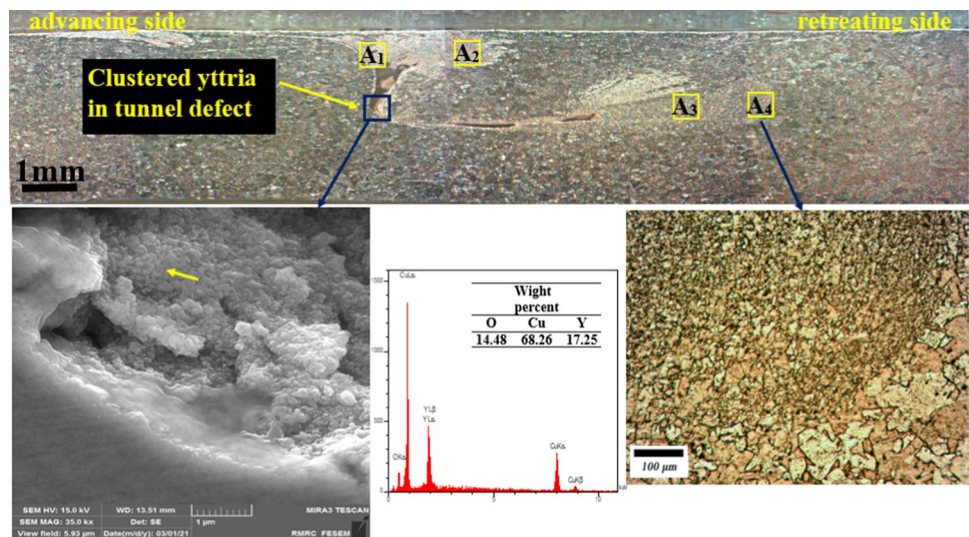

(a)
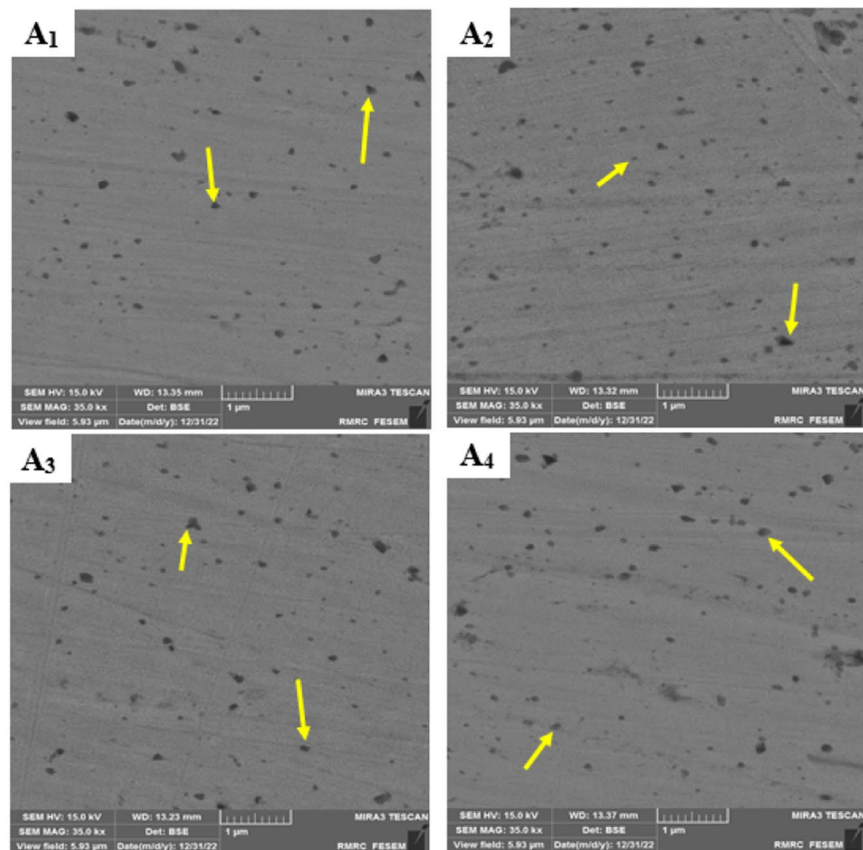
(b)

sample, which may have been due to its initial dislocation density. However, the elongation of the annealed sample after FSP was still higher than that of the processed CGPed sample because of a higher work hardening capacity. Adding nanoparticles reduced elongation in both annealed and CGP-treated samples.

3.7 Wear

The variation of the friction coefficient versus sliding distance during the pin-on-disk wear test is shown in Fig. 12. The SEM micrograph of the worn surfaces is depicted in Fig. 13. As can be seen in Fig. 12a, the friction coefficient

Fig. 5 (continued)

(c)

(a)

(b)
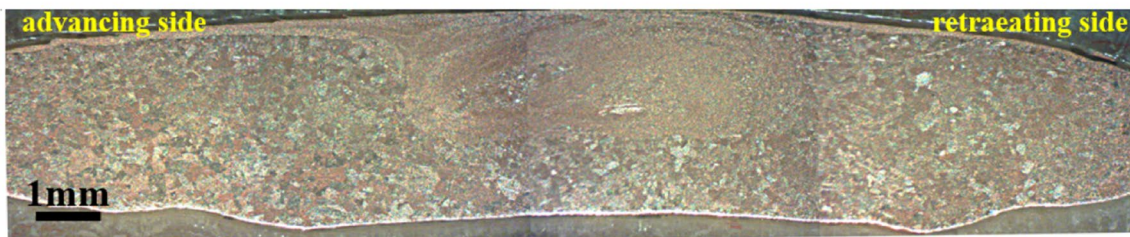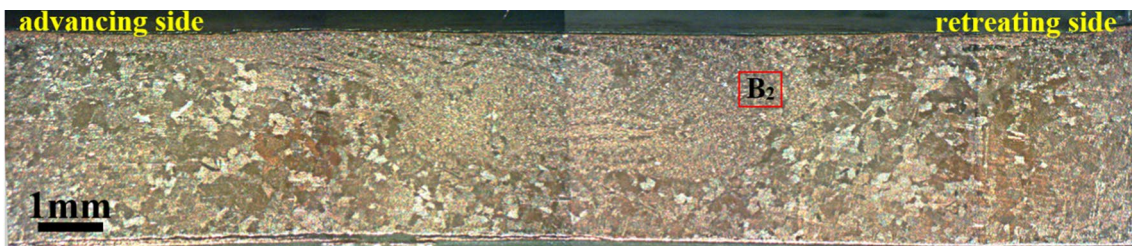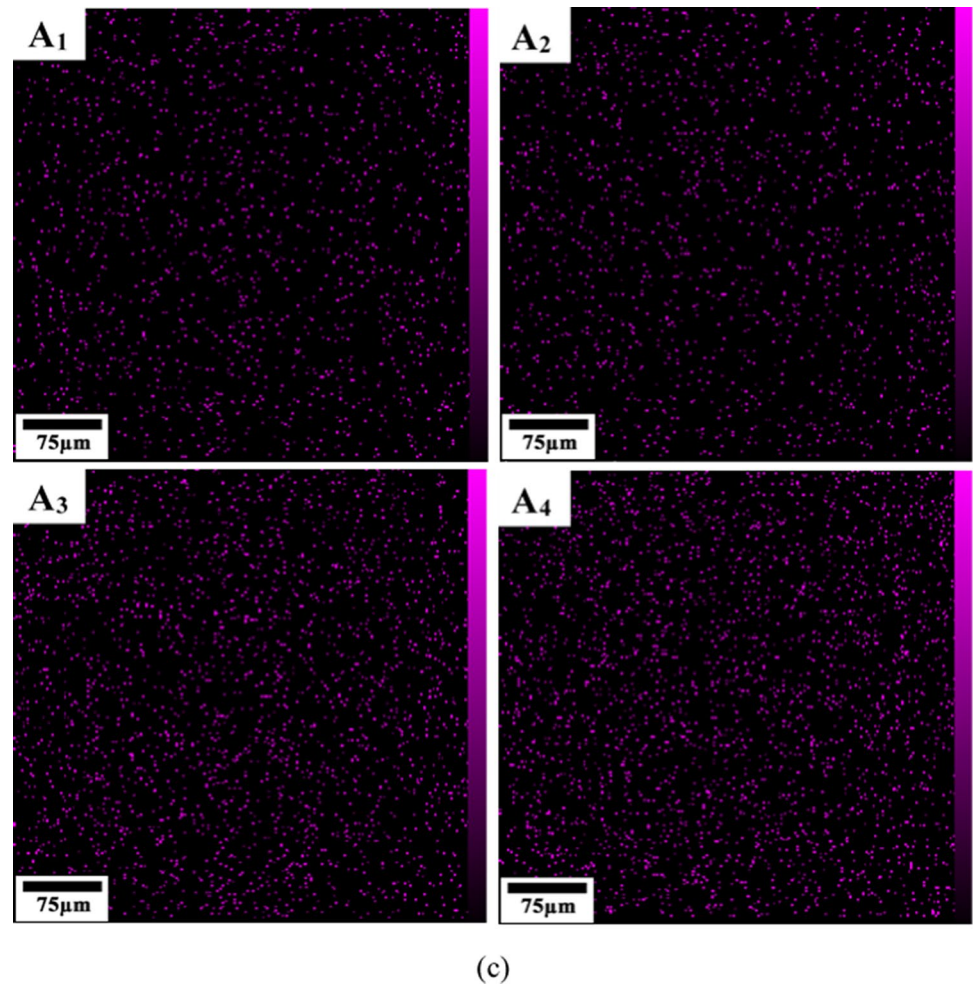
Fig. 6 Macrograph of the transverse cross-section of samples after 3-pass FSP, **a** annealed and **b** CGP-treated sample
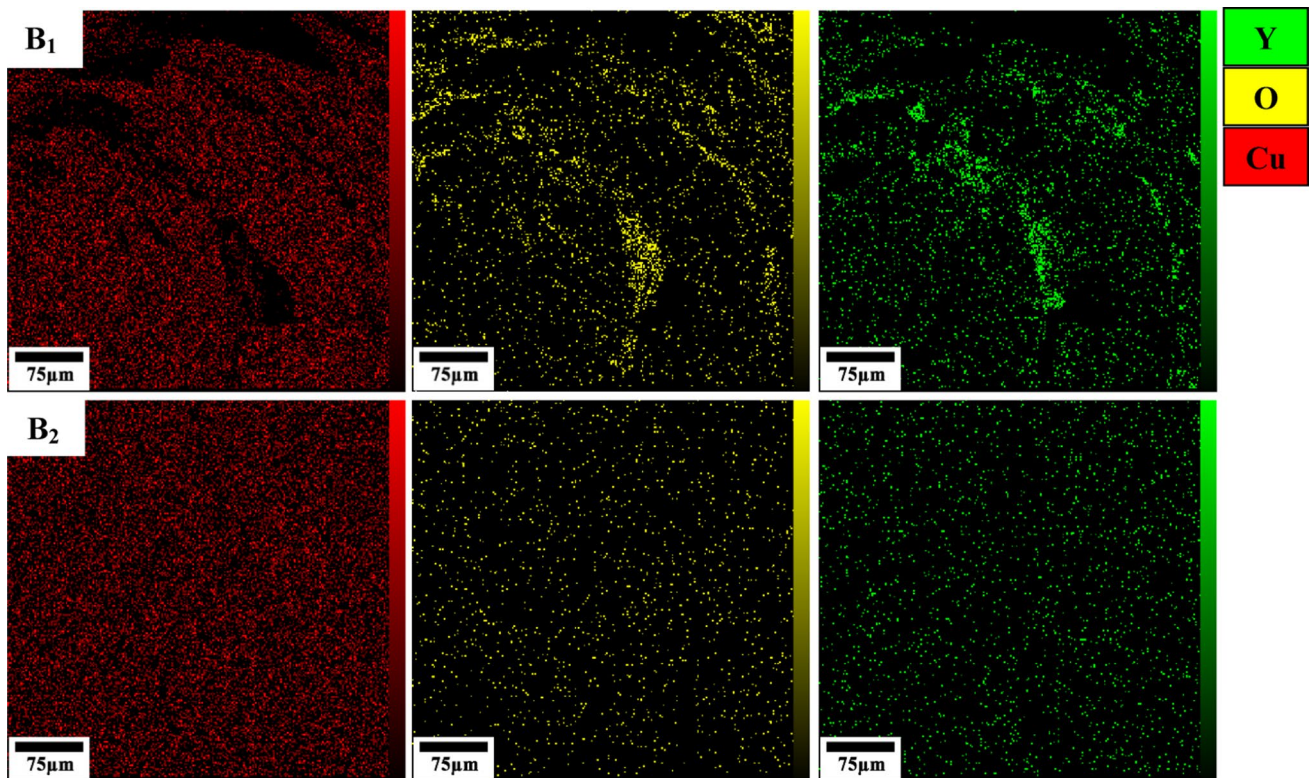
Fig. 7 EDX elemental map analysis of copper, oxygen and yttrium elements for B_1 and B_2 regions marked in Figs. 4a and 6a

Fig. 8 Microstructure of SZ for annealed specimens after **a** 1-pass FSP without Y_2O_3, **b** 3-pass FSP without Y_2O_3, **c** 1-pass FSP with Y_2O_3, and **d** 3-pass FSP with Y_2O_3
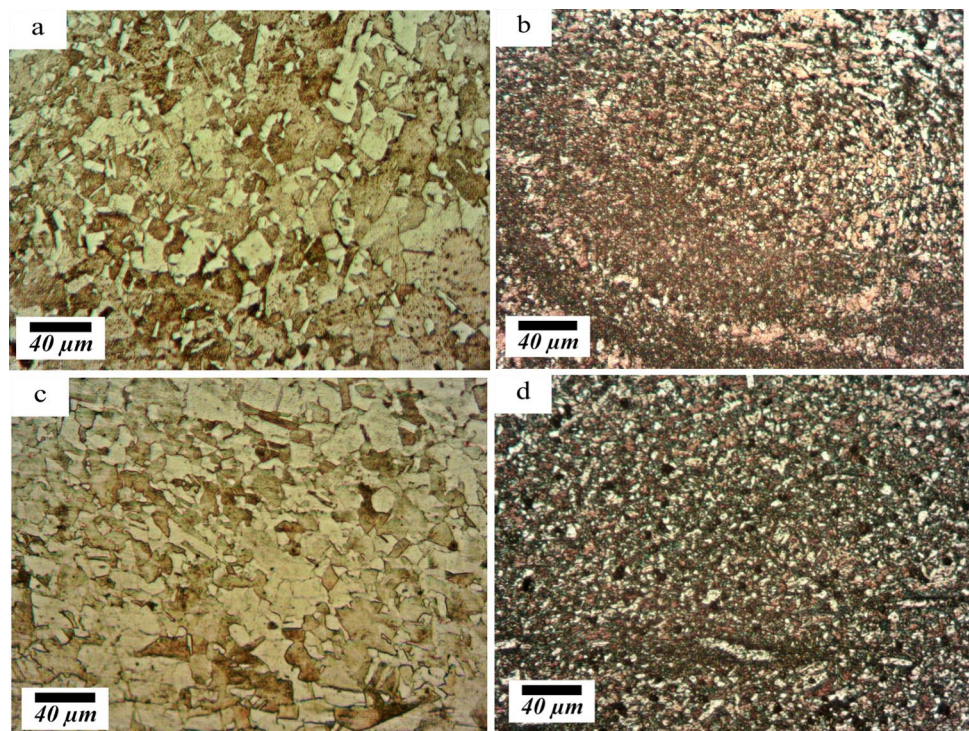
Fig. 9 Stir zone microstructure of severely deformed specimens after **a** 1-pass FSP without Y_2O_3, **b** 3-pass FSP without Y_2O_3, **c** 1-pass FSP with Y_2O_3, and **d** 3-pass FSP with Y_2O_3
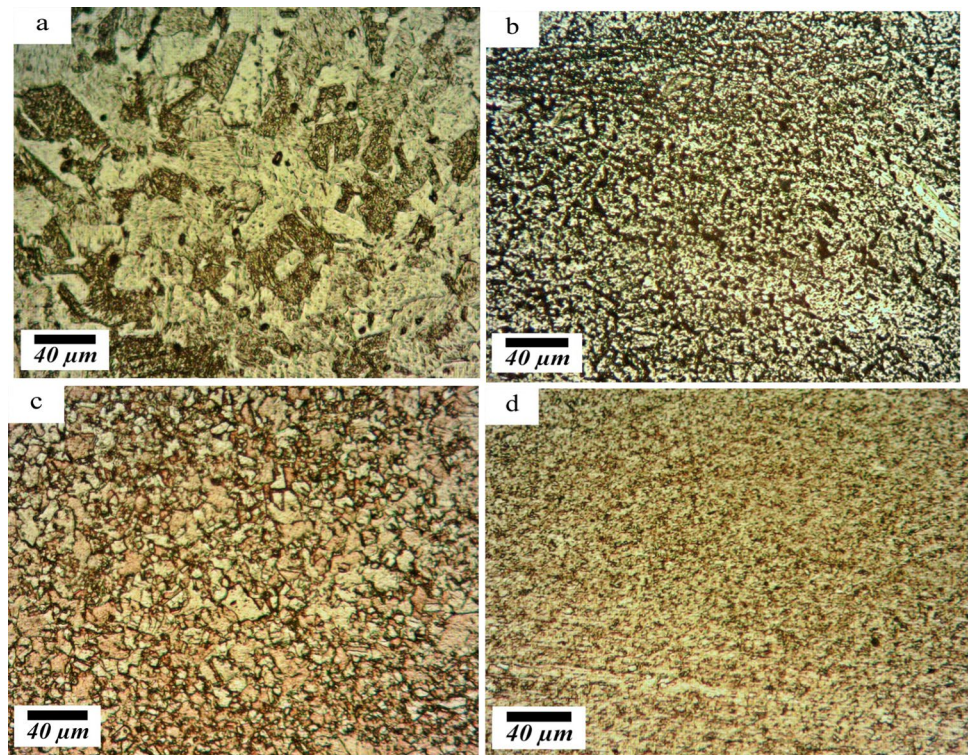

Table 1 Mean grain size of SZ after FSP of annealed and CGP processed samples, with and without yttria nanoparticles

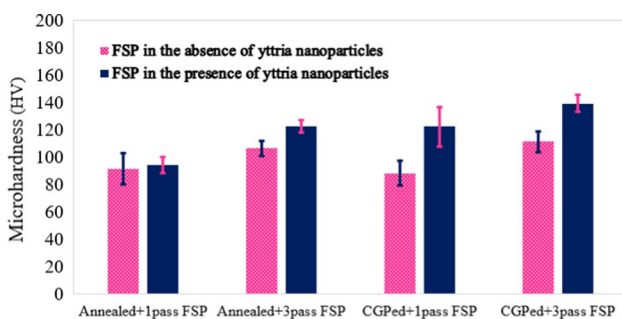| Specimen	Annealed without Y_2O_3 (μm)	Annealed with Y_2O_3 (μm)	CGP processed without Y_2O_3 (μm)	CGP processed with Y_2O_3 (μm)
1-pass FSP	12	13	28	4
3-pass FSP	3.8	3.2	2.1	1

Fig. 10 Stir zone hardness for the annealed and CGPed samples subjected to FSP in the presence and absence of yttria nanoparticles.

curve for the annealed sample after 1-pass FSP without particles experiences non-uniform fluctuations with a large amplitude, which is evidence of the adhesive wear mechanism [9]. Moreover, the worn surface micrograph of this

sample has the typical appearance of the adhesive wear mechanism. (Fig. 13a). Comparing Figs. 12a and b, it can be seen that by addition of the yttrium oxide nanoparticles, the amplitude of the fluctuations on the friction coefficient curve is reduced and its pattern becomes more uniform. In addition, the average friction coefficient decreased from 0.64 in the 1-pass FSPed samples without nanoparticles to 0.55 in the sample processed with nanoparticles. This behavior may have been due to the reduction of the actual contact area between the rubbing surfaces due to the presence of nanoparticles, which reduced the adhesive wear [9, 37]. As shown in Fig. 14, with the addition of nanoparticles to the annealed sample, the amount of weight loss was decreased from 2.1 to 1.8 mg because the nanoparticles increased the hardness and thus reduced the plastic deformation and wear rate [37].

According to Fig. 12c, the friction coefficient for the annealed sample treated by 3-pass FSP with nanoparticles increased compared to the 1-pass processed sample. As evident from Fig. 13c, during the wear test of the 3-pass FSPed sample, some microcracks were formed on the composite surface. The presence of nanoparticles may increase the rate of nucleation and propagation of cracks [37]. The delamination of the worn surface in the 3-pass processed sample resulted in a higher weight loss compared to the 1-pass processed specimen (Fig. 14). The results in Figs. 12d and 13d show that in the CGPed sample after 1-pass FSP, the adhesion between the rubbing surfaces decreased during the wear test, resulting in a
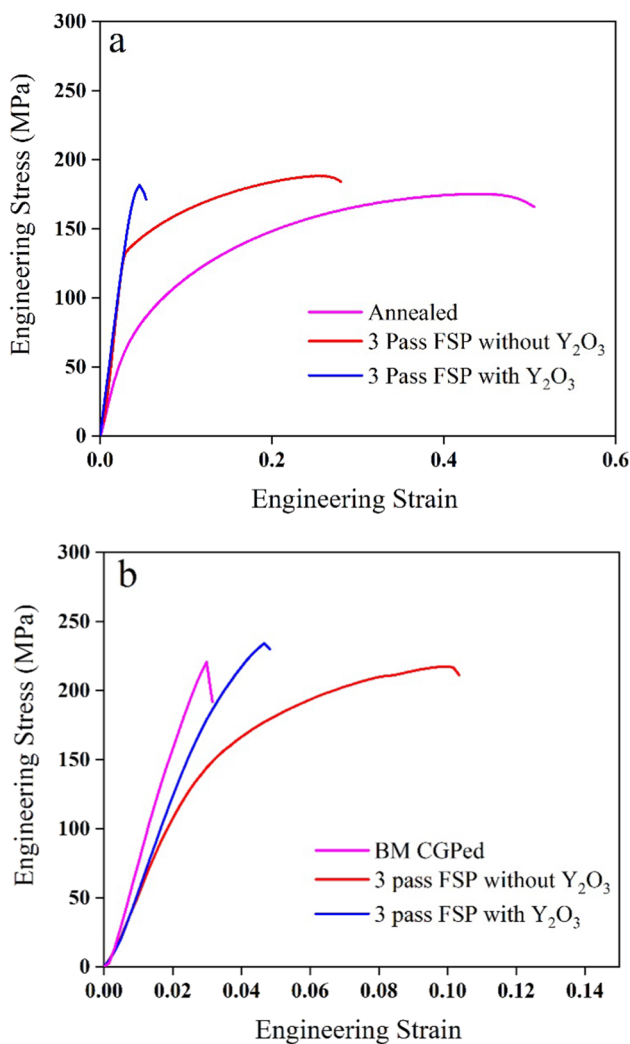
Fig. 11 Engineering stress–strain curves of SZ in 3-pass FSPed samples **a** annealed, and **b** CGP-treated

particles, in the CGP-treated sample, delamination of the worn surface due to the presence of a high fraction of nanoparticles led to the formation of a large number of debris (Fig. 13e). However, the amplitude of fluctuations in the friction coefficient curve (Fig. 12e) and the amount of weight loss (Fig. 14) for the 3-pass CGPed sample were lower than those of the annealed one. This could have been due to the higher hardness of the CGP-treated sample. The average coefficient of friction in the CGP-treated sample increased from 0.56 for the 1-pass treated specimen to 0.67 for the 3-pass FSPed one. The friction coefficient is directly related to the shear strength of the worn surface [37]. Due to the uniform dispersion of nanoparticles, the 3-pass processed sample experienced enhanced hardness and shear strength, which created a higher friction coefficient.

4 Conclusions

In this work, the influence of adding yttria nanoparticles during FSP on microstructure and mechanical properties of annealed and CGP-treated pure copper sheets was investigated. The main results are as follows:

1. By applying 4 passes of the CGP process on the annealed pure copper sheet, a fine grain structure with an average grain size of 7.7 μm, and a high hardness of about 2 times the initial value was achieved.
2. After 1-pass FSP without Y_2O_3 particles, the annealed sample showed a finer grain size with a higher hardness than the corresponding BM, while the SZ of the CGPed sample had a coarser grain with a lower hardness than the CGP-treated BM.
3. 1-pass FSP with yttria nanoparticles resulted in particle agglomeration in the SZ of the annealed sample with a small enhancement in hardness. However, the SZ hardness of the CGPed sample increased significantly compared to the sample processed without nanoparticles. Also, some tunnel defects were observed in the SZ of CGP-treated samples.

lower wear rate compared to the annealed samples. The finer grain size of the CGP-treated sample resulted in higher hardness and thus less weight loss than the annealed one. Similar to the annealed sample subjected to 3-pass FSP with yttria

Table 2 Tensile properties of BM and SZ for the annealed and CGP-treated samples processed by 3-pass FSP

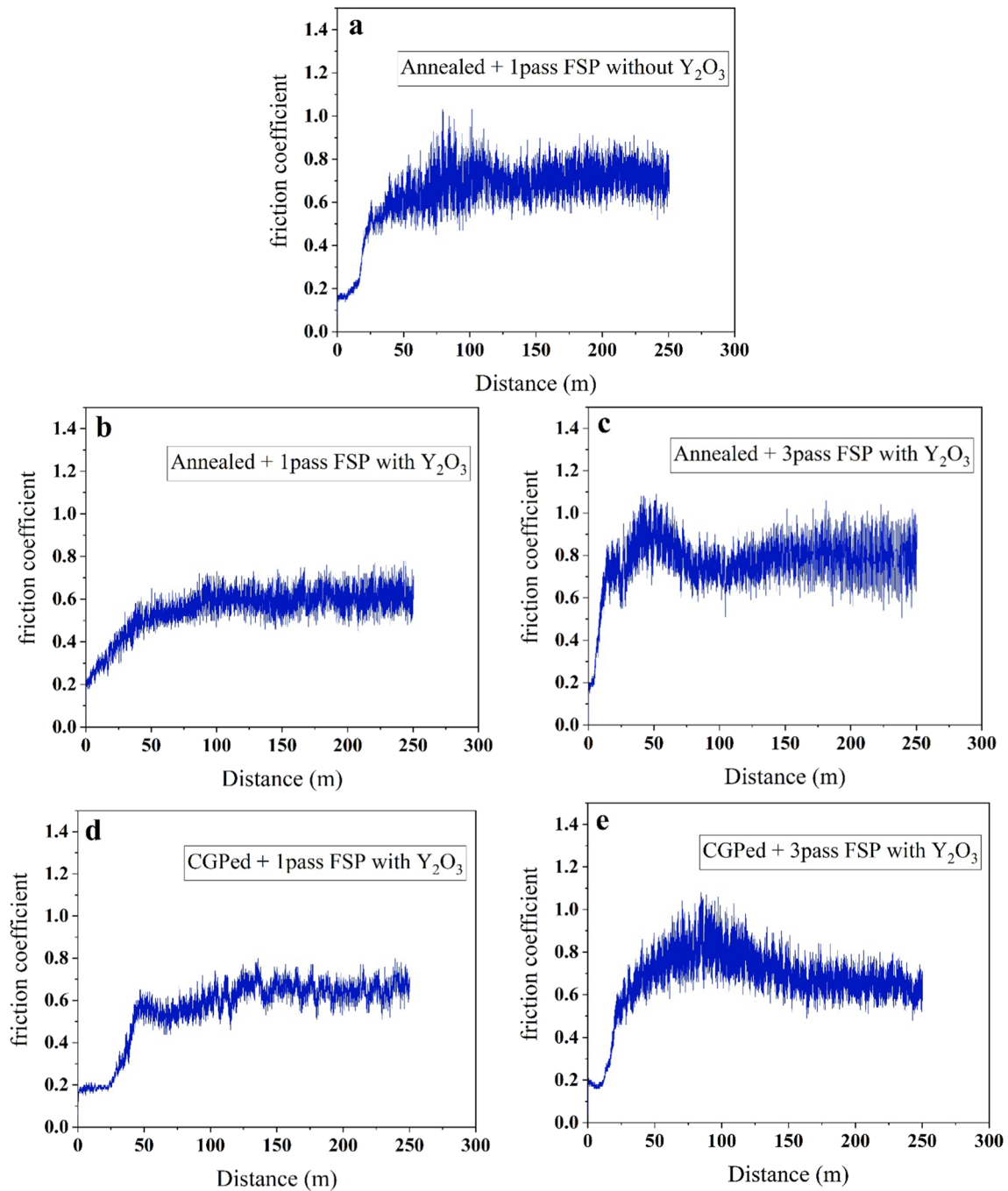| Samples	BM annealed	3-pass FSP without Y_2O_3	3-pass FSP with Y_2O_3	BM CGPed	3-pass FSP without Y_2O_3	3-pass FSP with Y_2O_3
σy (MPa)	52	106	116	144	101	153
UTS (MPa)	175	188	181	220	217	234
Elongation %	50	28	5.3	3	10	4.8

Fig. 12 Variation of friction coefficient vs sliding distance for **a** annealed + 1-pass FSP without nanoparticles, **b** annealed + 1-pass FSP with nanoparticles, **c** annealed + 3-pass FSP with nanoparticles, **d** CGP + 1-pass FSP with nanoparticles, and **e** CGP + 3-pass FSP with nanoparticles

4. Increasing the number of FSP passes resulted in a homogeneous distribution of particles in the SZ with finer grain size and higher hardness value in annealed and CGP-treated samples.

5. The annealed sample after 3-pass FSP with nanoparticles showed a small improvement in YS, with a slight decrease in UTS, and a relatively large reduction in elongation, compared to the 3-pass FSPed sample with-

Fig. 13 SEM images of the worn surfaces for **a** annealed + 1pass FSP without nanoparticles, **b** annealed + 1 pass FSP with nanoparticles, **c** annealed + 3 passes FSP with nanoparticles, **d** CGP + 1 pass FSP with nanoparticles, and **e** CGP + 3 passes FSP with nanoparticles
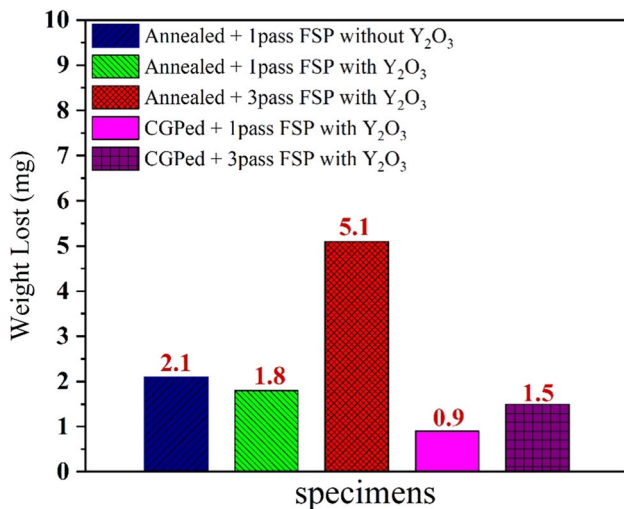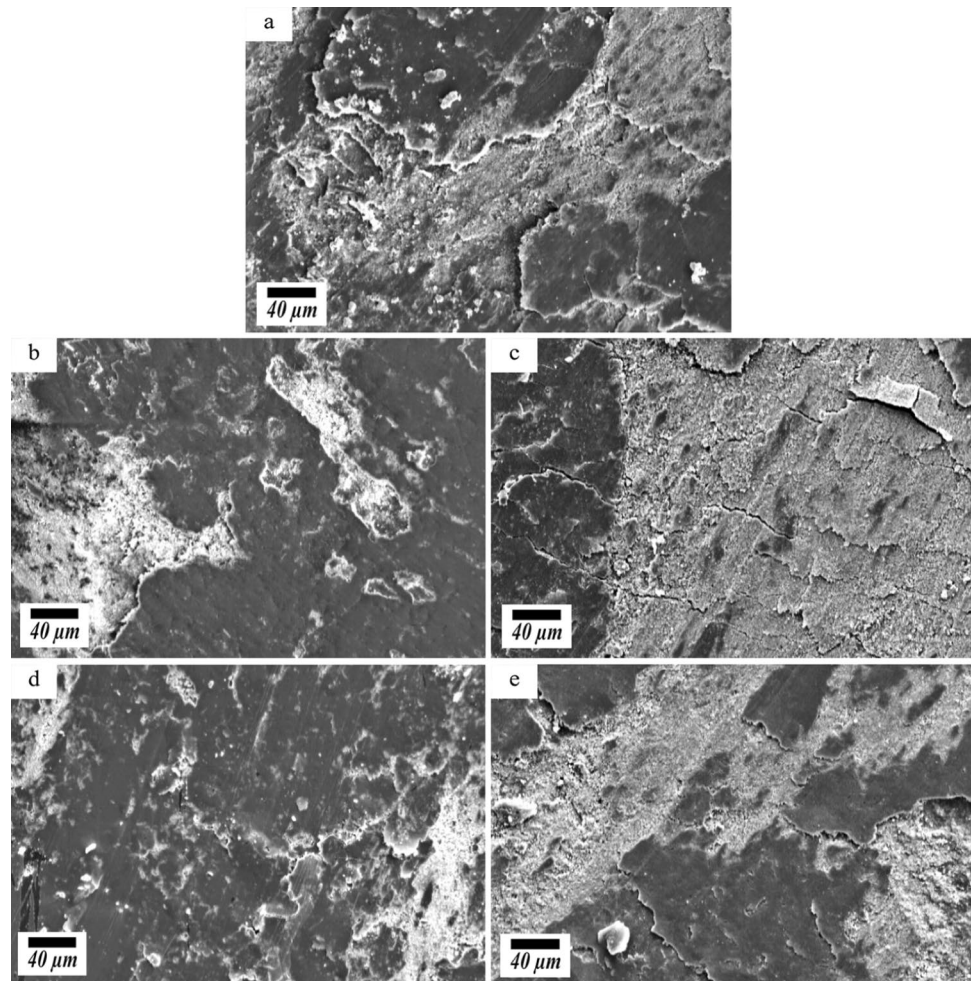

Fig. 14 Weight loss for the annealed and CGP-treated samples during wear test with sliding distance of 250 m

out particles. While the strength of the CGPed sample increased after 3-pass FSP with nanoparticles compared to the CGP-treated BM.

6. By adding yttria nanoparticles to the annealed sample during 1-pass FSP, the average friction coefficient and the amount of weight loss decreased compared to the sample FSPed without particles, while with a higher number of FSP passes, the friction coefficient and the amount of weight loss increased significantly. The CGP-treated sample experienced minimal weight loss after 1-pass FSP. By increasing the number of FSP passes in the CGPed sample, the average friction coefficient and the weight loss increased. In all conditions, the CGPed samples experienced less weight loss than the annealed samples.

Data Availability The raw/processed data required to reproduce these findings cannot be shared at this time due to legal or ethical reasons.

Declarations

Conflict of Interest The authors declare that there is no conflict of interest.

References

1. R.Z. Valiev, R.K. Islamgaliev, I.V. Alexandrov, Bulk nanostructured materials from severe plastic deformation. Prog. Mater. Sci. **45**, 103–189 (2000)
2. D.H. Shin, J.-J. Park, Y.-S. Kim, K.-T. Park, Constrained groove pressing and its application to grain refinement of aluminum. Mater. Sci. Eng. A **328**, 98–103 (2002)
3. S.C. Yoon, A. Krishnaiah, U. Chakkingal, H.S. Kim, Severe plastic deformation and strain localization in groove pressing. Comput. Mater. Sci. **43**, 641–645 (2008)
4. A. Krishnaiah, U. Chakkingal, P. Venugopal, Applicability of the groove pressing technique for grain refinement in commercial purity copper. Mater. Sci. Eng. A **410–411**, 337–340 (2005)
5. Z.S. Wang, Y.J. Guan, P. Liang, Deformation efficiency, homogeneity, and electrical resistivity of pure copper processed by constrained groove pressing. Rare Met. **33**, 287–292 (2014)
6. B. Mohammadi, M. Tavoli, F. Djavanroodi, Effects of constrained groove pressing (CGP) on the plane stress fracture toughness of pure copper. Struct. Eng. Mech. **52**, 957–969 (2014)
7. A.K. Gupta, T.S. Maddukuri, S.K. Singh, Constrained groove pressing for sheet metal processing. Prog. Mater. Sci. **84**, 403–462 (2016)
8. M. Barmouz, M.K.B. Givi, J. Seyfi, On the role of processing parameters in producing Cu/SiC metal matrix composites via friction stir processing: investigating microstructure, microhardness, wear and tensile behavior. Mater. Charact. **62**, 108–117 (2011)
9. M. Barmouz, M.K.B. Givi, Fabrication of in situ Cu/SiC composites using multi-pass friction stir processing: evaluation of microstructural, porosity, mechanical and electrical behavior. Compos. A Appl. Sci. Manuf. **42**, 1445–1453 (2011)
10. L.S. Raju, A. Kumar, Influence of Al_2O_3 particles on the microstructure and mechanical properties of copper surface composites fabricated by friction stir processing. Def. Technol. **10**, 375–383 (2014)
11. M. Sabbaghian, M. Shamanian, H.R. Akramifard, M. Esmailzadeh, Effect of friction stir processing on the microstructure and mechanical properties of Cu–TiC composite. Ceram. Int. **40**, 12969–12976 (2014)
12. H.R. Akramifard, M. Shamanian, M. Sabbaghian, M. Esmailzadeh, Microstructure and mechanical properties of Cu/SiC metal matrix composite fabricated via friction stir processing. Mater. Des. **54**, 838–844 (2014)
13. J. Khosravi, M.K.B. Givi, M. Barmouz, A. Rahi, Microstructural, mechanical, and thermophysical characterization of Cu/WC composite layers fabricated via friction stir processing. Int. J. Adv. Manuf. Technol. **74**, 1087–1096 (2014)
14. B.W. Ahn, J.H. Kim, K. Hamad, S.B. Jung, Microstructure and mechanical properties of a B4C particle-reinforced Cu matrix composite fabricated by friction stir welding. J. Alloys Compd. **693**, 688–691 (2017)
15. I. Dinaharan, S. Saravanakumar, K. Kalaiselvan, S. Gopalakrishnan, Microstructure and sliding wear characterization of Cu/TiB$_2$ copper matrix composites fabricated via friction stir processing. J. Asian Ceram. Soc. **5**, 295–303 (2017)
16. I. Dinaharan, R. Sathiskumar, N. Murugan, Effect of ceramic particulate type on microstructure and properties of copper matrix composites synthesized by friction stir processing. J. Mater. Res. Technol. **5**, 302–316 (2016)
17. M.-N. Avettand-Fènoël, A. Simar, R. Shabadi, R. Taillard, B. de Meester, Characterization of oxide dispersion strengthened copper based materials developed by friction stir processing. Mater. Des. **60**, 343–357 (2014)
18. Y.S. Sato, Y. Kurihara, S.H.C. Park, H. Kokawa, N. Tsuji, Friction stir welding of ultrafine grained Al alloy 1100 produced by accumulative roll-bonding. Scripta Mater. **50**, 57–60 (2004)
19. M. Lipińska, L. Olejnik, A. Pietras, A. Rosochowski, P. Bazarnik, J. Goliński, T. Brynk, M. Lewandowska, Microstructure and mechanical properties of friction stir welded joints made from ultrafine grained aluminium 1050. Mater. Des. **88**, 22–31 (2015)
20. W. Wang, K. Qiao, J.L. Wu, T.Q. Li, J. Cai, K.S. Wang, Fatigue properties of friction stir welded joint of ultrafine-grained 2024 aluminium alloy. Sci. Technol. Weld. Join. **22**, 110–119 (2017)
21. H. Fujii, R. Ueji, Y. Takada, H. Kitahara, N. Tsuji, K. Nakata, K. Nogi, Friction stir welding of ultrafine grained interstitial free steels. Mater. Trans. **47**, 239–242 (2006)
22. M.S. Khorrami, M. Kazeminezhad, A.H. Kokabi, Mechanical properties of severely plastic deformed aluminum sheets joined by friction stir welding. Mater. Sci. Eng. A **543**, 243–248 (2012)
23. H. Barekatain, M. Kazeminezhad, A.H. Kokabi, Microstructure and mechanical properties in dissimilar butt friction stir welding of severely plastic deformed aluminum AA 1050 and commercially pure copper sheets. J. Mater. Sci. Technol. **30**, 826–834 (2014)
24. I. Topic, H.W. Höppel, M. Göken, Friction stir welding of accumulative roll-bonded commercial-purity aluminium AA1050 and aluminium alloy AA6016. Mater. Sci. Eng. A **503**, 163–166 (2009)
25. M.S. Khorrami, M. Kazeminezhad, A.H. Kokabi, Influence of stored strain on fabricating of Al/SiC nanocomposite by friction stir processing. Metall. Mater. Trans. A **46**, 2021–2034 (2015)
26. M.S. Khorrami, M. Kazeminezhad, A.H. Kokabi, The effect of SiC nanoparticles on the friction stir processing of severely deformed aluminum. Mater. Sci. Eng. A **602**, 110–118 (2014)
27. M.S. Khorrami, M. Kazeminezhad, Y. Miyashita, N. Saito, A.H. Kokabi, Influence of ambient and cryogenic temperature on friction stir processing of severely deformed aluminum with SiC nanoparticles. J. Alloys Compd. **718**, 361–372 (2017)
28. C. Hamilton, S. Dymek, M. Blicharski, A model of material flow during friction stir welding. Mater. Charact. **59**, 1206–1214 (2008)
29. N. Soni, S. Chandrashekhar, A. Kumar, V.R. Chary, defects formation during friction stir welding: a review. Int. J. Eng. Manag. Res. **7**, 121–125 (2017)
30. X. Hou, X. Yang, L. Cui, G. Zhou, Influences of joint geometry on defects and mechanical properties of friction stir welded AA6061-T4 T-joints. Mater. Des. **53**, 106–117 (2014)
31. F.J. Humphreys, M. Hatherly, *Recrystallization and Related Annealing Phenomena* (Pergamon Press, Oxford, 2004)
32. M. Barmouz, M.K. Besharati Givi, J. Jafari, Evaluation of tensile deformation properties of friction stir processed pure copper: effect of processing parameters and pass number. J. Mater. Eng. Perform. **23**, 101–107 (2014)

33. N. Xu, R. Ueji, H. Fujii, Enhanced mechanical properties of 70/30 brass joint by multi-pass friction stir welding with rapid cooling. Sci. Technol. Weld. Join. **20**, 91–99 (2015)

34. M. Zohoor, M.K.B. Givi, P. Salami, Effect of processing parameters on fabrication of Al–Mg/Cu composites via friction stir processing. Mater. Des. **39**, 358–365 (2012)

35. H. Kumar, M.Z. Khan, M. Vashista, Microstructure, mechanical and electrical characterization of zirconia reinforced copper based surface composite by friction stir processing. Mater. Res. Express. **5**, 86505 (2018)

36. G. Purcek, O. Saray, M.I. Nagimov, A.A. Nazarov, I.M. Safarov, V.N. Danilenko, O.R. Valiakhmetov, R.R. Mulyukov, Microstructure and mechanical behavior of UFG copper processed by ECAP following different processing regimes. Philos. Mag. **92**, 690–704 (2012)

37. J. Zhu, L. Liu, B. Shen, W. Hu, Mechanical properties of Cu/SiCp composites fabricated by composite electroforming. Mater. Lett. **61**, 2804–2809 (2007)